THz RADIATION SOURCE THROUGH PERIODICALLY MODULATED STRUCTURES

PROF. DR. ERICH GORNIK

INSITUT FÜR FESTKÖRPERELEKTRONIK
TECHNISCHE UNIVERSITÄT WIEN
FLORAGASSE 7
A- 1040 WIEN
GERMANY

CONTRACT NO. N68171-96-C-9015
RDD 7372-EE-01

8 th Interim Report

September 1997- November 1997

REPORT DOCUMENTATION PAGE

Form Approved
OMB NO. 0704-0188

1. AGENCY USE ONLY *(Leave blank)*	2. REPORT DATE	3. REPORT TYPE AND DATES COVERED
	December 4, 1997	Interim, July 1997 - November 1997

4. TITLE AND SUBTITLE

THz Radiation Source Trough Periodically Modulated Structures

5. FUNDING NUMBERS

C
N 68171-96-C-9015

6. AUTHOR(S)

E. Gornik, Ch. Rauch, G. Strasser, K. Unterrainer, R. Kersting

7. PERFORMING ORGANIZATION NAMES(S) AND ADDRESS(ES)

Institut für Festkörperelektronik
Technische Universität Wien
Floragasse 7
A-1040 Wien, Austria

8. PERFORMING ORGANIZATION REPORT NUMBER

8th Interim Report

9. SPONSORING / MONITORING AGENCY NAME(S) AND ADDRESS(ES)

U.S. Army Research Office
P.O. Box 12211
Research Triangle Park, NC 27709-2211

10. SPONSORING / MONITORING AGENCY REPORT NUMBER

WK2Q6C-7372-EE01

11. SUPPLEMENTARY NOTES

The views, opinions and/or findings contained in this report are those of the author(s) and should not be construed as an official Department of the Army position, policy or decision, unless so designated by other documentation.

12a. DISTRIBUTION / AVAILABILITY STATEMENT

Approved for public release; distribution unlimited.

12 b. DISTRIBUTION CODE

13. ABSTRACT *(Maximum 200 words)*

The work on the developement of new injection structures was continued. These experiments demonstrate the transition from coherent transport to band like scattering induced transport in a superlattice miniband. A mean free path of an injected electron in the order of 75 nm can be estimated for our ten period superlattices by using the experimental results for coherent and incoherent current at a fixed negative bias of 20 meV. This bias value corresponds exactly to the miniband width. Thus the onset of the Bloch oscillation regime appears at the value predicted by the Esaki-Tsu model. In the next period of the project we will manufacture individual bow-tie antennas coupled to the small mesas to enhance the emitted radiation. This step is also necessary for the other emission devices which are grown to demonstrate THz emission from plasma instabilities.

We have observed THz emission from coherent plasma oscillations vertical to the surface of bulk semiconductors.The THz emission results from the response of carriers to the field screening induced by the ultrafast photoexcitation. Carriers are accelerated vertically to the surface and perform coherent oscillations around their new equilibrium state which leads to the emission of THz radiation. Our time-resolved measurements of the THz emission give insight into the dynamics of these plasma oscillations and their generation processes.

14. SUBJECT TERMS

Carrier injection, quantum wires, THz sources, superlattice spectroscopy

15. NUMBER IF PAGES

16. PRICE CODE

17. SECURITY CLASSIFICATION OR REPORT	18. SECURITY CLASSIFICATION OF THIS PAGE	19. SECURITY CLASSIFICATION OF ABSTRACT	20. LIMITATION OF ABSTRACT
UNCLASSIFIED	UNCLASSIFIED	UNCLASSIFIED	UL

REPORT DOCUMENTATION PAGE (SF298)
(Continuation Sheet)

8th Interim Report

Transition between coherent and incoherent electron transport in semiconductor superlattices

The work on the developement of new injection structures was continued. In the process of this work a breakthrough in the understanding of electric field driven superlattice transport was achieved. For the first time the transition between coherent and incoherent transport in GaAs/AlGaAs superlattices is observed. The previously described three terminal device is used to probe the transmittance of undoped GaAs/$Ga_{0.7}Al_{0.3}As$ superlattices. The measured collector current reflects the probability of an injected electron to be transmitted through the superlattice. The transmittance of the superlattice can be measured directly at given superlattice bias conditions by varying the injected current independently from the superlattice bias voltage.

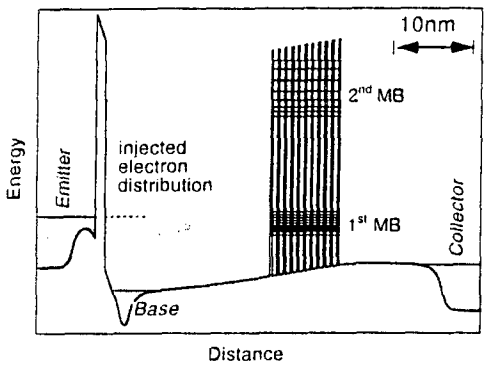

Figure 1: Schematic band diagram of a three terminal device with negative bias applied to the superlattice.

Two superlattice structures were investigated consisting of either 5 or 10 periods of 2.5 nm $Ga_{0.7}Al_{0.3}As$ barriers and 6.5 nm GaAs wells. The calculated conduction band energy diagram including band bending is shown in Fig. 1 for typical biasing conditions.

The static transfer ratio $\alpha=I_C/I_E$ is measured as a function of negative emitter bias (=injected electron energy) at 4.2 K in a common base configuration. In Fig. 2 the transfer ratio α versus injection energy of the ten period superlattice is shown for different collector biases. The black solid line represents the transfer ratio at flat band condition ($U_{BC}=0$). A clear shift of the maximum and a reduction of the amplitude of the transfer ratio is observed for negative collector voltages while after an increase a significant lower reduction of the amplitude and of the shift is observed for increasing positive collector biases. The five period superlattice shows a symetric dependence of the peak value of the transfer ratios for both bias directions.

The analysis of the total miniband transmission, T_α, versus applied electric field for both superlattices is shown in Fig. 3. The total miniband transmission T_α of the five period sample (dots) is symmetric for both bias directions, while an asymmetric behavior is observed for the ten period sample (squares). The experimental datas are compared to calculation based on a transfer matrix method. The calculation for the five period superlattice

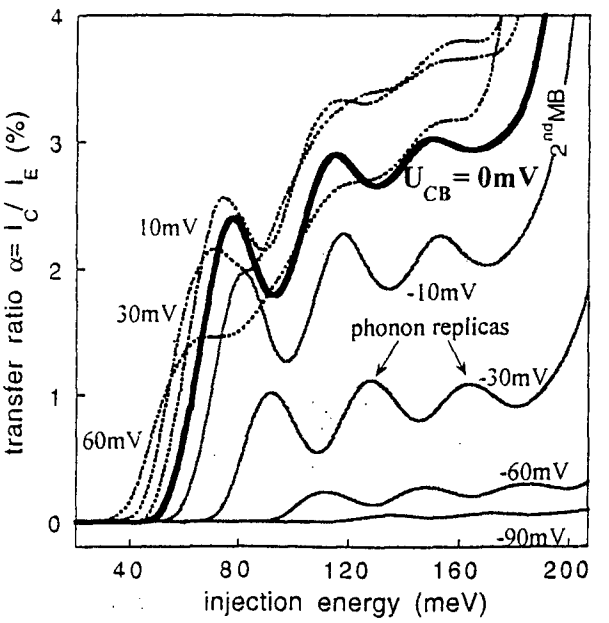

Figure 2: Transfer ratio α versus injection energy at different collector base voltages of the ten period sample.

agrees quite well with the experiment, demonstrating that the transport through a five period superlattice (total length 45 nm) is coherent for all electric fields. No difference is found between an accelerating and decelerating electric field which is in agreement with the theory of coherent transport. There is no evidence for significant scattering induced current.

However, the picture changes dramatically for the ten period structure: For negative bias (decelerating field) the measured current decays much faster with field than the calculated coherent current. For positive bias the current first increases slightly until it decays rapidly but always stays higher than the calculated current. We assign the observed difference between the ten and five period superlattice to the onset of scattering induced miniband transport. For the ten period superlattice a considerable fraction of the carriers does not traverse the superlattice without scattering. In the positive bias case we observe an increase of the transfer ratio since the scattered electrons contribute additionally with the coherent electrons to the collector current. For the negative bias case we assume that only coherent electrons traverse the superlattice, scattered electrons are flowing back to the base according to the applied field.

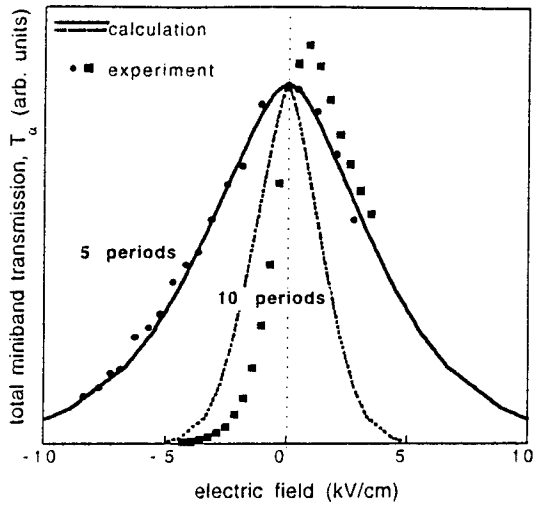

Figure 3: The total miniband transmission versus electric field. The calculation (solid and dashed line) is based on a transfer matrix method.

These experiments demonstrate for the first time the transition from coherent transport to band like scattering induced transport in a superlattice miniband. We can estimate the additional scattering induced current as a function of superlattice bias by subtracting the measured coherent part from the experimental result as shown in Fig. 4. For that we have to assume that the coherent transport is also symmetric for positive and negative bias for the ten period superlattice which is very well justified from the results of the five period superlattice. After a weakly linear increase a well defined maximum in the incoherent current is observed for an electric field value around 1.6 kV/cm. A mean free path of an injected electron in the order of 75 nm can be estimated for our ten period superlattices by using the experimental results for coherent and incoherent current at a fixed negative bias of 20 meV (Fig.3). This bias value corresponds exactly to the miniband width. Thus the onset of the Bloch oscillation regime appears at the value predicted by the Esaki-Tsu model.

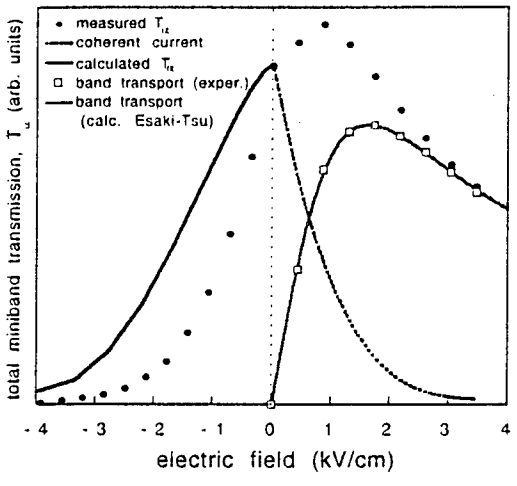

Figure 4: Total miniband transmission versus electric field of the ten period superlattice. For positive applied bias, coherent (dashed line) and incoherent current (squares) is present. The incoherent current is fitted using the Esaki-Tsu formula (Eg. 2). For negative bias the experimental result is well below the calculated coherent current (solid line), indicating scattering induced losses in the collector current.

We have observed for the first time the transition between resonant tunneling and band transport in a solid state using vertical tunneling through biased semiconductor superlattices. The band transport is induced by scattering and overcomes the localization of the electron wave functions introduced by an applied electric field.

Development of THz emission devices

According to the results on coherent transport in superlattices (coherence length = 75 nm) we believe that Bloch oscillations are possible since scattering is weak enough in our superlattices. At 20 mV bias we have a situation where 10 % of the carriers traverse the superlattice without scattering. This situation can lead to Bloch type oscillations for a certain fraction of the carriers. This is what we believe is observed in the experiment described above where the current drops drastically with increasing electric field.. By making the length of the superlattice close to the mean free path we match the conditions for Bloch oscillations.

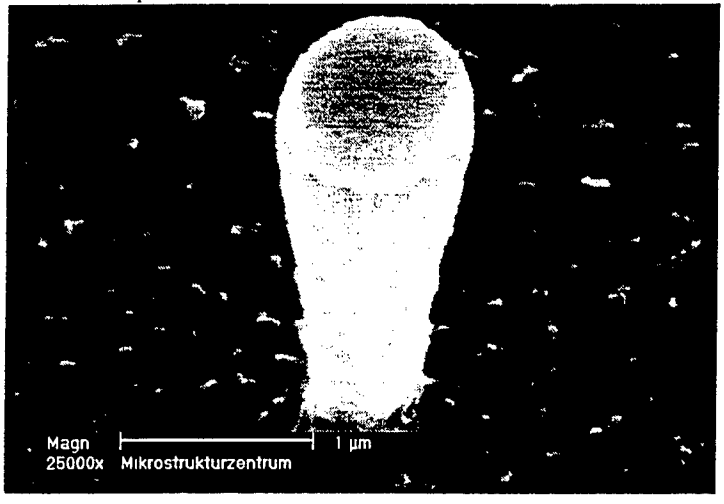

Figure 5: SEM picture of a dry etched 1 μm^2 Mesa. AuGeNi is used serves as an ohmic contact and as an etch mask.

To enhance the emission output of such superlattices, small mesas are fabricated and coupled to coplanar broad band bow-tie antenna. The superlattice mesas with an area of 1 μm^2 (Fig. 5) are formed by dry etching. The top and bottom highly doped n^+ -GaAs contact layers are connected via airbridges to the bow-tie antenna in order to avoid undesired parasitic capacities. The airbridges are fabricated by electro plating on top of a photosensitive Polyimid layer.

In the next period of the project we will manufacture individual bow-tie antennas coupled to the small mesas to enhance the emitted radiation. This step is also necessary for the other emission devices which are grown to demonstrate THz emission from plasma instabilities.

Few cycle Thz-emission form plasma oscillation on semiconductors

Since the first observation of THz emission from semiconductor surfaces excited by ultrafast laser pulses, considerable effort has been made both in understanding the mechanism responsible for the THz generation, and in applications of these few-cycle THz pulses. Besides THz generation by Bloch-oscillations, two processes are discussed leading to the emission of THz--radiation in bulk semiconductors. One is the instantaneous polarization that arises during optical excitation when electron-hole pairs are generated in the electric field region of a semiconductor as for example, in the depletion or surface field. A second emission process results from the transport of photoexcited carriers in the field region. The first process is attributed to coherent effects during optical excitation and the latter to the motion of carriers which includes ballistic transport and carrier drift.

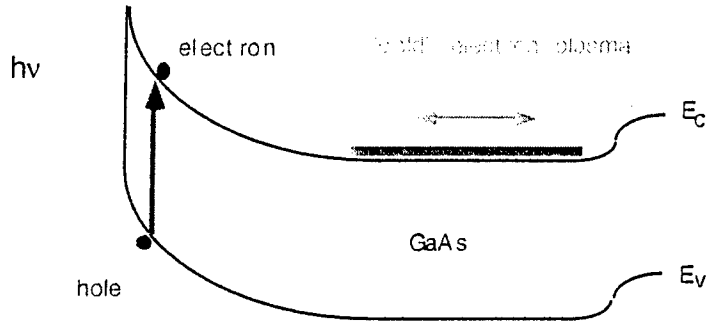

Figure 6: THz generation process

We have observed THz emission from coherent plasma oscillations vertical to the surface of bulk semiconductors. The THz emission results from the response of carriers to the field screening induced by the ultrafast photoexcitation. Carriers are accelerated vertically to the surface and perform coherent oscillations around their new equilibrium state which leads to the emission of THz radiation. The basic scheme is sketched in Fig. 6. Our time-resolved measurements of the THz emission give insight into the dynamics of these plasma oscillations and their generation processes. A fundamentally new emission process is found in n-doped bulk GaAs. The THz emission results from the response of cold carriers to the dynamic field screening induced by hot photogenerated carriers.

All experiments are performed using a mode-locked Ti:Sapphire laser emitting 100 fs pulses at 800 nm (1.55 eV) with a pulse energy of 13 nJ. The pulses are transmitted through a Michelson interferometer and focused onto the sample. In the reflection geometry, the generated THz emission is collected by off-axis parabolic mirrors and focused onto a 4.2 K bolometer. Appropriate filtering is used to eliminate the contribution from the red pump light. The experimental setup is purged with nitrogen to prevent absorption by atmospheric humidity. The signal is detected using standard lock-in techniques at a modulation frequency of about 400 Hz. Time resolution is achieved in our experiment by focusing two delayed laser pulses on the sample which are generated by the Michelson interferometer. In this correlation technique the time integrated THz-signal emitted from the sample is detected with the bolometer as a function of the delay time between the two exciting pulses. Assuming only partial field screening of the first exciting pulse, the second also generates an oscillating polarization. Since these polarizations are superimposed at the bolometer, the detected cw-signal depends on the phase between the oscillations which is given by the time delay between the two exciting laser pulses.

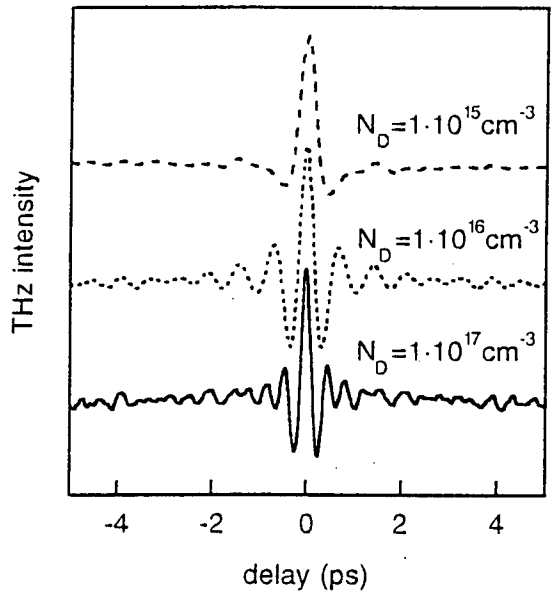

Fig. 7: THz correlation data recorded on n-doped GaAs-structures. The excitation density is always smaller than the doping concentration.

The n-doped samples were grown on semi-insulating substrates with epilayer thicknesses of 3.7 μm, 2.0 μm, and 1.8 μm. The doping densities n_D are determined by standard Hall measurements

and are corrected for the depletion layer thickness yielding concentrations of $1.9 \cdot 10^{15} cm^{-3}$, $1.7 \cdot 10^{16} cm^{-3}$, and $1.1 \cdot 10^{17} cm^{-3}$, respectively.

Time-resolved data from these samples are shown in Fig. 7. Multiple oscillations are clearly visible at higher doping concentrations. The oscillation period depends only on the doping concentration and does not show any dependence on the density of photogenerated carriers.

In Fig. 8 the coressponding Fourier transform spectra are shown. The peak frequency shifts to higher frequency for increasing carrier concentration. The observed oscillation frequencies correspond very well to the plasma frequency $\omega_P = \sqrt{\frac{n_D e^2}{m^* \varepsilon}}$, where n_D is the doping concentration, and m* is the effective mass.

We explain the experimental results in the following framework. In n-doped structures cold electrons are confined by the surface depletion on one side and by the electric field at the interface between the epilayer and the substrate on the other side. In the initial stage the hot photoexcited carriers screen the surface field. This also leads to a field change beyond the depletion zone in the bulk of the sample. Here, the field change accelerates the cold electrons which subsequently undergo plasma oscillations due to the restoring force of the ionized impurities.The plasma frequency is given by the density of the cold electrons. Since the field change beyond the depletion zone is small the amplitude of the resulting plasma oscillations is also small having an important consequence for the damping of these oscillations.

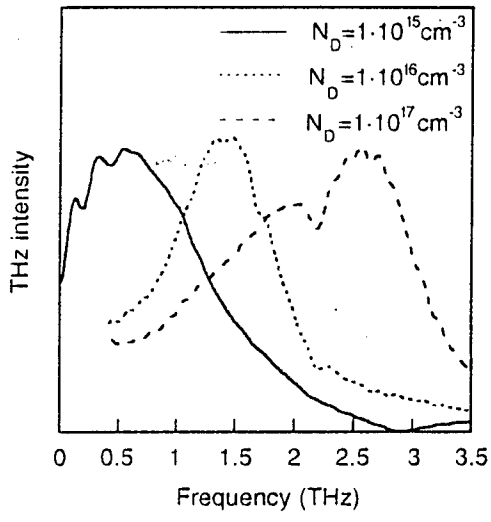

Fig. 8: Corresponding Fourier spectra.

We assume that plasma damping by LO phonon scattering of the electrons is the dominant damping mechanism. We compared our measured damping times to the electron-optical phonon rates, which can be estimated from the DC mobility. The DC-scattering rates agree with the values of the plasmon damping very well which suggests that phonon scattering is the dominant damping mechanism of the cold plasma oscillations.

The damping also limits the emission power of the plasma oscillation. Damping reduces the density of coherently oscillating carriers and their dipole moment. Thus, the plasma frequency and the emitted power are strongly reduced in the case of short damping times. Therefore, cold plasma oscillations in n-doped structures offer an attractive approach to generate efficiently few-cycle THz pulses. Our measured emission intensities confirm this. The emission power of the n-doped samples is up to 2 orders of magnitude higher than the power emitted from p-i-n structures.